



ARTICLE OPEN



Hailstorms and rainstorms versus supercells—a regional analysis of convective storm types in the Alpine region

Monika Feldmann^{1,2}, Alessandro Hering², Marco Gabella² and Alexis Berne¹

The behaviour of severe thunderstorms, particularly supercells, in complex terrain is still poorly understood. Utilising 6 years of radar-, lightning- and radiosounding-based thunderstorm data in the domain of the Swiss radar network, we study different thunderstorm types in separate topographical regions. We classify the storms as ordinary thunderstorms, intense and severe rainstorms, hail and severe hailstorms and supercellular storms. After identifying the overlaps between the storm categories of rainstorms, hailstorms and supercells, the life cycles of several intensity metrics are investigated. This analysis allows the identification of predictors for intensification within severe storm life cycles. One of the most important predictors is the detection of a mesocyclone in a supercell before the onset or intensification of hail. We then divide the radar domain into sub-regions ranging from the Northwestern Po Valley, the Southern Prealps, main Alpine ridge, Northern Prealps, Swiss Plateau and Jura. This regional split separates storms in different terrain complexities. An investigation of the intensity distribution of storms in each region shows a clear intensity decrease over the main Alpine ridge, intermediate values over the moderately complex Prealpine regions and peaks for the flat Po Valley and Swiss Plateau. In contrast, the highest frequency of storms is found in the Prealpine regions on each side, with a lower frequency in the flat areas and a minimum in convective activity over the main Alpine ridge.

npj Climate and Atmospheric Science (2023)6:19; <https://doi.org/10.1038/s41612-023-00352-z>

SEVERE THUNDERSTORMS

Severe thunderstorms are one of the most costly natural hazards^{1–3}. They can lead to straight-line winds, intense rainfall, large hail and even tornadoes⁴. These phenomena pose a risk to infrastructure, properties and human life. With the fraction of severe thunderstorms expected to increase with climate change in Europe^{5–8}, improved understanding of severe thunderstorms is highly relevant for future risk assessment.

Research on severe thunderstorms often focuses on single hazards, such as studies on hail^{9–13} or severe rain^{14–17}. We here aim to take a more comprehensive approach and study multiple aspects of severe convection across diverse topographic regions. To improve short-term warnings, nowcasting hail and precipitation has been a priority in Europe^{15,18–22}. Key findings have been the integration of orographic enhancement in precipitation nowcasting^{18,21,23} and considering lightning jumps for hail^{20,24}.

While severe thunderstorms have been studied for a long time, there is still limited understanding about their behaviour in complex terrain. Several studies on hailstorms in Switzerland^{11,24–26} discuss their occurrence and behaviour in the Alpine region. Previous studies on supercell thunderstorms in Switzerland^{27–29} show their overlap with and similarity to severe hailstorms. Analyses in Germany have shown comparisons between mesocyclonic and non-mesocyclonic storms^{20,30} and also discuss the life cycle of hailstorms^{31,32}. They show that lightning jumps generally precede the most intense hail in a storm's life cycle, which was also shown for Switzerland in ref. ²⁴. In addition, in most cases, mesocyclonic storms will produce the mesocyclone before or with the onset of hail^{30,33,34}. Numerous studies focus on single severe storms in or near complex terrain in Europe^{35–43}, in the USA^{44–46} and South America^{47,48}. A broader stance is taken in several studies^{49–51}, where clusters of severe thunderstorms causing large hail and flash floods in central Europe are analysed. Studies in Italy investigate the conditions

leading to tornadoes throughout the country⁵², as well as the distribution of lightning in the Northeastern region ranging from the Adriatic coast to the Julian Alps⁵³. In Austria, a multi-year assessment of severe convection in radar and reanalysis data investigated the dependency of convective organisation on atmospheric shear⁵⁴. More recent studies in the United States⁵⁵ and Argentina⁵⁶ also focus on severe convection in more complex terrain utilising large, multi-year event sets. In addition, the dependency of storm environments on topography in the Eastern USA is presented in ref. ⁵⁷. A multi-sensor-based climatology for thunderstorms in Europe is provided in ref. ⁵⁸.

With the United States experiencing some of the most severe convection worldwide, numerous studies focus on this region. The research ranges from investigating hailstorms in remote sensing data⁵⁹ to establishing climatologies of hail^{60,61}, quasi-linear convective systems⁶² and mesoscale convective systems⁶³, as well as analysing the changing trends in tornado and hail occurrence^{64,65}.

Utilising data sets from lightning networks and severe weather reports, a comparison between severe convection climatologies in Europe and the United States was established⁶⁶. Consequently, the differences in regional trends in the past decades were discussed⁶⁷, with modelled severe convective environments in Europe increasing, while they are decreasing in the United States. A more global stance is taken in ref. ⁶⁸, where differences in globally observed convective trends are highlighted.

In this study, we provide a comprehensive comparison of severe thunderstorm types, by comparing ordinary thunderstorms to severely precipitating storms, hailstorms and supercellular thunderstorms in the Alpine region. We particularly focus on the behaviour of supercell thunderstorms, whose behaviour in complex terrain is still poorly understood. The comparison to other, better-understood convective storm types provides the necessary context. Each of these storm categories are classified

¹Environmental Remote Sensing Laboratory, EPFL, Lausanne, Switzerland. ²Radar, Satellites and Nowcasting Division, MeteoSwiss, Switzerland. ✉email: monika.feldmann@epfl.ch

using radar-based metrics and can overlap with each other. We highlight the differences in the life cycles between the severe convective storm types. By dividing the Alpine region into sub-regions of homogeneous topographical complexity, we dissect the different behaviours of severe convection in comparison to the orography. Establishing a thunderstorm classification from the same radar-based data set over different orographic regions allows for a direct comparison of both storm types in general and the differences in the orographic regions. Previous studies usually only allow for comparison either between storm types in less complex terrain, or highlight the distribution of one storm type in different terrain situations, thus only inferring indirect comparisons.

RESULTS

Classifying convective storms with radar-based criteria

This study is based on radar-derived thunderstorm data from the extended convective season running from April to October of the years 2016–2021 in Switzerland. The Swiss radar domain is shown in Fig. 1. With five C-band Doppler dual-polarisation radars situated at altitudes from 900 m ASL to ~2900 m ASL, the network covers a large portion of the Alps, extending into France, Italy, Austria and Germany, as well as the surrounding Prealpine regions and plains^{69,70}. Each radar scans a full volume of 20 elevations every 5 min. From the 100 polar elevation scans at a resolution of 500 m × 1°, 2-D merged Cartesian products at a 1 km spatial resolution are derived. Consequently, the thunderstorm data set has a spatial resolution of 1 km and a temporal resolution of 5 min.

In addition, the available radio-sounding data from the observational sites in Payerne (Swiss Plateau) and Milano (NW Po Valley)

were extracted during the observation period (2491 soundings from Payerne and 2463 from Milano⁷¹). The soundings are performed twice per day at 00:00 and 12:00 UTC.

Figure 1a shows a topographical map of the analysed region, indicating the radar locations and names. The polygons show the regional split into areas of differing homogeneous topographical complexity. They largely follow the polygons used in refs. ⁷² and ²⁵. Table 1 shows an overview of the regions. A relative quality index (QI) for radar data (derived in ref. ²⁹) is shown in Fig. 1b, which ranges from 0 (relatively lowest observational quality in the network) to 1 (relatively highest observational quality). We exclude all areas below 0.3 QI (teal-hatched areas) to avoid quality biases in the radar data. A further discussion of the influence of radar quality is provided in Supplementary Discussion 1.

Our observational domain is split into six regions. To the South of the Alps, where the Northwestern (NW) Po valley and the Southern (S) Prealps are located, the weather regime is Mediterranean with favourable convective environments. The main Alpine ridge serves as a weather divide. To the North of the Alps the regions Northern (N) Prealps, Swiss Plateau and Jura experience a central European weather regime. Additional information on the regional weather regimes is provided in Supplementary Discussion 2.

The data set of thunderstorms contains tracked thunderstorms, using the Thunderstorm Radar Tracking (TRT) algorithm^{73,74}, lasting at least 30 min that are identified with unique IDs. For each thunderstorm, several intensity metrics are gathered from the operational radar data⁷⁰, lightning detection network^{75–77}, radiosoundings⁷¹ and numerical weather prediction model COSMO-1⁷⁸. The most relevant storm metrics used for this study are listed in Table 2. As almost all analysed variables in this study

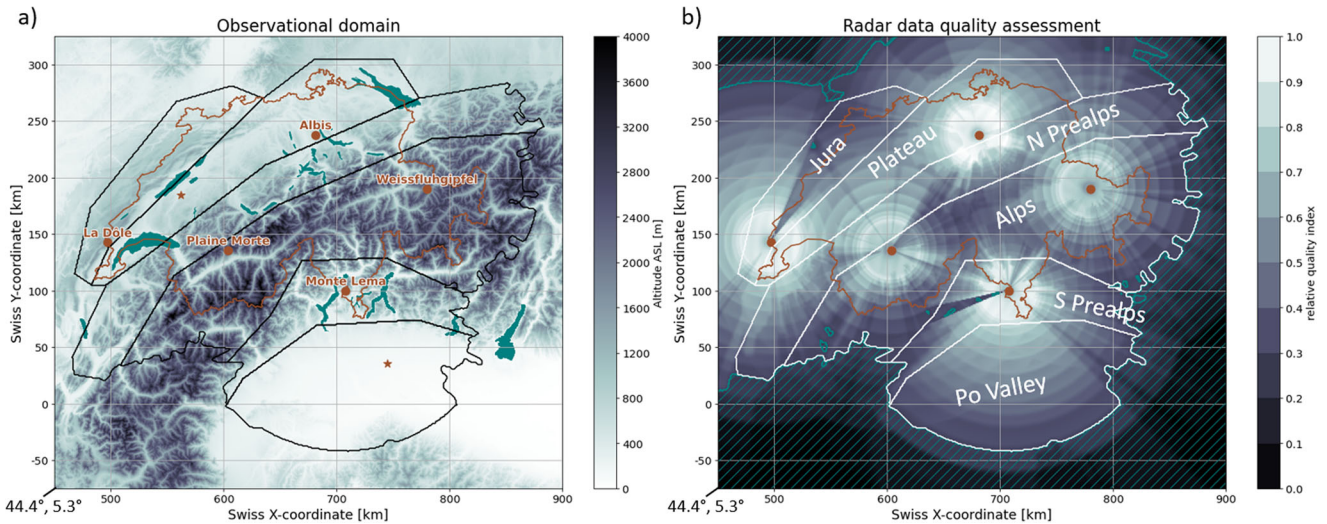


Fig. 1 Topography and data quality in the observational domain. a Radar domain and regional split, underlain with topographical elevation map (Digital elevation model from refs. ⁹⁹ and ¹⁰⁰), as well as site of the five radars in Switzerland (dots) and two sounding sites (stars); **b** relative quality index of radar observations for convective phenomena²⁹ and regional split with regions' names.

Table 1. Description of regions.				
Region	Topography	Weather regime	Area (km ²)	Average QI \bar{Q}
Northwestern (NW) Po valley	Flat	Mediterranean	17,862	0.47
Southern (S) Prealps	Smaller mountain chains	Mediterranean	9887	0.60
Central Alps (Alps)	High mountain terrain	Mixed, Alpine	31,110	0.51
Northern (N) Prealps	Smaller mountain chains	Central European	17,764	0.58
Swiss Plateau (Plateau)	Hills	Central European	14,347	0.71
Jura	Smaller mountain chains	Central European	8448	0.57

are derived from radar data, we show the correlation between all considered variables in Supplementary Discussion 3.

These thunderstorms are further divided into hail (HS) and severe hailstorms (SHS), based on criteria on the probability of hail

Acronym	Definition	Unit
A	Storm area	km ²
A57dBz	Storm area with reflectivity ≥ 57 dBz	km ²
LTG	Cloud-to-ground (CG) lightning	# (5 min A) ⁻¹
RANK	Heuristic thunderstorm severity rank (see Eq. (1))	[unitless, 0–40]
ET45	45 dBz echo top height	km ASL
ACC	Radar-derived precipitation accumulation in last hour	mm h ⁻¹
iRR	Radar-derived instantaneous precipitation rate	mm h ⁻¹
VIL	Vertically integrated liquid	kg m ⁻²
Z	Cartesian composite maximum radar reflectivity	dBz
Zmax	Maximum Z within A	dBz
MESHS	Maximum expected severe hail size	cm
POH	Probability of hail	%
v	Translational speed	km h ⁻¹

(POH) and maximum expected severe hail size (MESHS), rain (RS) and severe rainstorms (SRS), based on criteria of hourly accumulated precipitation (ACC), supercells (SC), with a detected mesocyclone, and ordinary thunderstorms (OR) that meet none of the previous criteria. The complete tracks assigned to the previously defined regional polygons and the life cycles are centred around the time T0 they first meet their storm-type classification. A summary of classification criteria, region assignment and the definition of T0 is found in Table 3. A more detailed explanation of these methods can be found in “Methods”.

Occurrence frequency of different convective types

To get an overview of the frequency of different thunderstorm types, we first investigate their overall occurrence. The following Fig. 2 shows the total number of detected storm tracks per category and the overlap of the hazard categories.

The majority of all detected thunderstorms are OR, occurring more than one order of magnitude more frequently than the next most frequent category of RS. RS and SRS occur slightly more frequently than HS or SHS. SC are the least frequent thunderstorm type with 540 detected tracks among 73,688 total analysed thunderstorm tracks.

When looking at the overlap between RS and SRS, HS and SHS and SC, here shown with a Venn diagram, the majority of SC are also classified as HS or RS. RS and HS also overlap considerably, but there are larger fractions with a single hazard. SRS are not necessarily characterised by other hazardous features. Relatively weak, but

Class	Criterion	Region anchor	Centre of life cycle
Ordinary (OR)	<4 contiguous* km ² of POH >80% or MESHS >2 cm; <3 cont.* km ² of ACC >30 mm h ⁻¹ ; no mesocyclone	Most frequent region Weighted by intensity	Highest intensity
Rainstorm (RS)	>= 3 contiguous* km ² of ACC >30 mm h ⁻¹	Most frequent region during intense rain	Intense rain onset
Severe rainstorm (SRS)	>= 3 contiguous* km ² of ACC >50 mm h ⁻¹	Most frequent region during severe rain	Severe rain onset
Hailstorm (HS)	>= 5 contiguous* km ² of POH >80% or MESHS >2 cm	Most frequent region during hail	Hail onset
Severe hailstorm (SHS)	>= 5 contiguous* km ² of MESHS >4 cm	Most frequent region during severe hail	Severe hail onset
Supercell (SC)	Classified by mesocyclone detection algorithm	Most frequent region during mesocyclones	Mesocyclone onset

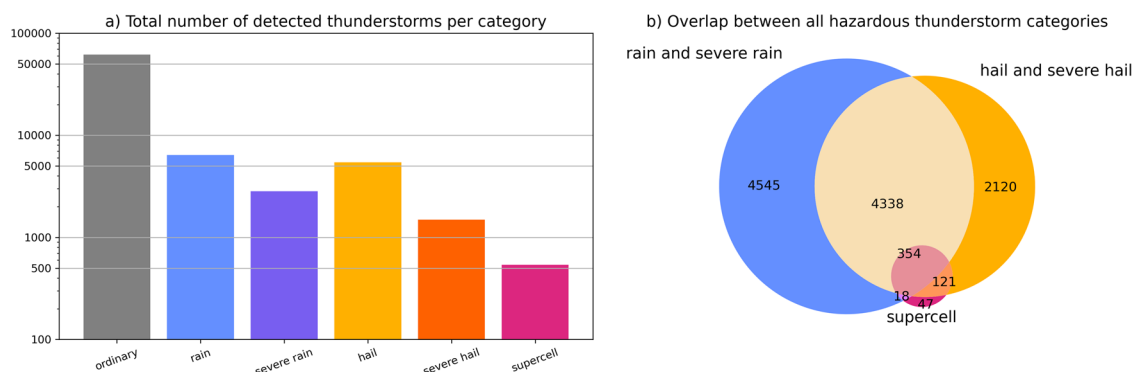


Fig. 2 Overall occurrence of different convective types. **a** Number of detected storms per category, **b** overlap between hazardous thunderstorm categories—rain and severe rain, as well as hail and severe hail are each categorised together, over the entire 6-year data set.

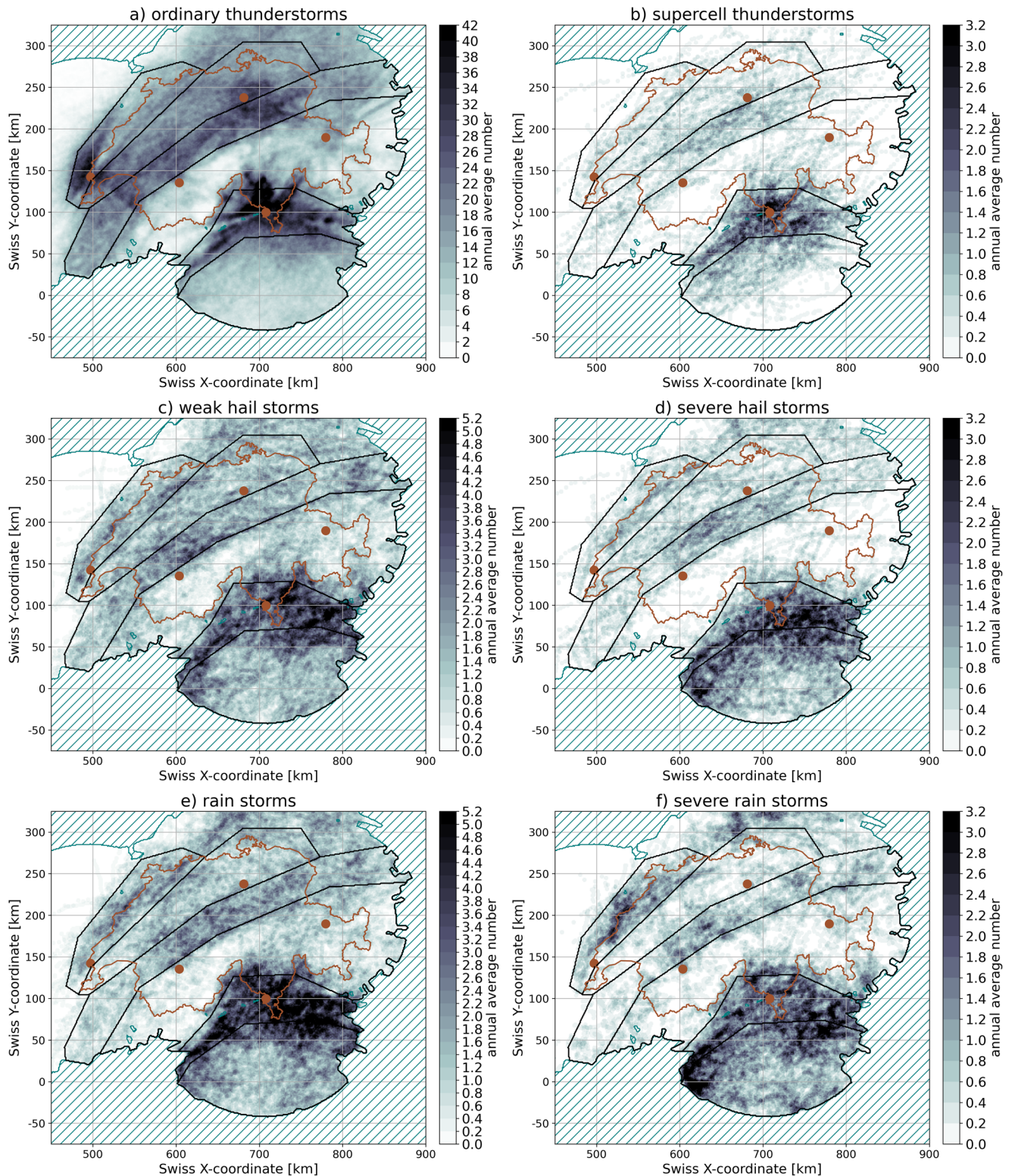


Fig. 3 Annual average spatial occurrence of each thunderstorm type (2016–2021). **a** Ordinary thunderstorms, **b** supercell thunderstorms, **c** weak hailstorms, **d** severe hailstorms, **e** rainstorms, **f** severe rainstorms; greyscale differs across figure panels. The sites of the five radars are also indicated, as well as the regional polygon boundaries.

stationary thunderstorms can precipitate intensely enough to trigger the rain accumulation threshold. While the majority of all SC are also HS, the inverse is not true. Out of all SHS, only ~10% present with a mesocyclone. This differs from the results of ref. ³¹, where the majority of SHS present with a mesocyclone. So while

SHS still occur regularly in the complex topography of Switzerland^{11,13,24,25,79}, the conditions of SC are less prevalent and they occur less frequently²⁹.

Next, we show the average annual spatial distribution per thunderstorm type in Fig. 3. Each thunderstorm detection is

depicted with a radius of 5 km, corresponding to a localised storm density. A single storm can contribute to more than one category. Beginning with OR, we can clearly see the climatology and the influence of the radar data quality (see Fig. 1b). Particularly, our ability to observe weak thunderstorms of small spatial and vertical extent is impeded in areas of reduced radar visibility. More severe storm types tend to be taller and wider (see Fig. 4), leading to more robust detections even in lower-quality areas.

The overall pattern shows that the activity maximum for all convective storm types lies in the S Prealps, encroaching onto the NW Po valley^{11,79,80}. The N Prealps and Jura also show elevated activity, but less pronounced than the S Prealps. The Plateau has slightly reduced activity. The lowest overall activity is in the main Alpine ridge. The minimum in convective activity here is confirmed by satellite- and lightning-based climatologies that are independent of the radar network^{79,81–83}. This suggests that moderately complex terrain is beneficial to the formation of convection, whereas the high Alpine environment is detrimental^{79,80}.

Life cycles of different convective types

Investigating the life cycles of different convective types allows us to better understand their defining characteristics. By analysing their behaviour before and during their most intense phases, we can gain insight into the processes related to hazardous weather phenomena.

In Fig. 4, we show the 45 min prior to the life cycle anchoring point of each storm type, as well as the hour after. This encompasses the expected lifetime of most convective storms, as well as the usual useful time frame of less than an hour for thunderstorm nowcasting purposes. If we observe distinct behaviour leading up to the anchor,

this variable may have predictive and thus nowcasting properties. We show the evolution of the median, as well as the 25th and 75th quantiles (shaded areas) for each convective storm type. We focus on the variables severity rank [unitless] (see Eq. (1)), area [km^2], translational speed [km h^{-1}], CG lightning strikes [$\# (5 \text{ min } A)^{-1}$], MESHS [cm] and iRR [mm h^{-1}]. The translational speed (computed from the distance of a thunderstorm's centroids in between timesteps) is considered an environmental variable, as it is determined by the storm's environment⁸⁴, whereas the others are storm-internal intensity variables.

Overall, we can see that both SHS and SC show the highest values in RANK, A, LTG, MESHS and iRR and longest lasting peaks during their life cycles. Most life cycle curves peak shortly before or at the life cycle anchor for all variables, apart from translational speed.

As determined by the definition of T0, OR peak in intensity at T0. Overall they have a lower intensity than all other storm types, but an intermediate translational speed.

In comparison, RS and SRS show slower translational speeds. The importance of stationary storms to heavy convective precipitation events has been analysed in more detail in ref. ¹⁶. Precipitation accumulation is driven by two factors, precipitation rate and precipitation duration. The more stationary a storm is, the longer it will precipitate over a given area, increasing the likelihood of exceeding the accumulation threshold. As they are classified by hourly precipitation accumulation, the processes in the hour preceding T0 are very important. We can see that the intensity variable peaks (most notably iRR) lie in the 30 min before T0, with a higher, broader and slightly earlier peak for SRS.

The life cycles of HS and SHS are quite similar in terms of the overall tendencies, but SHS experience higher and more prolonged

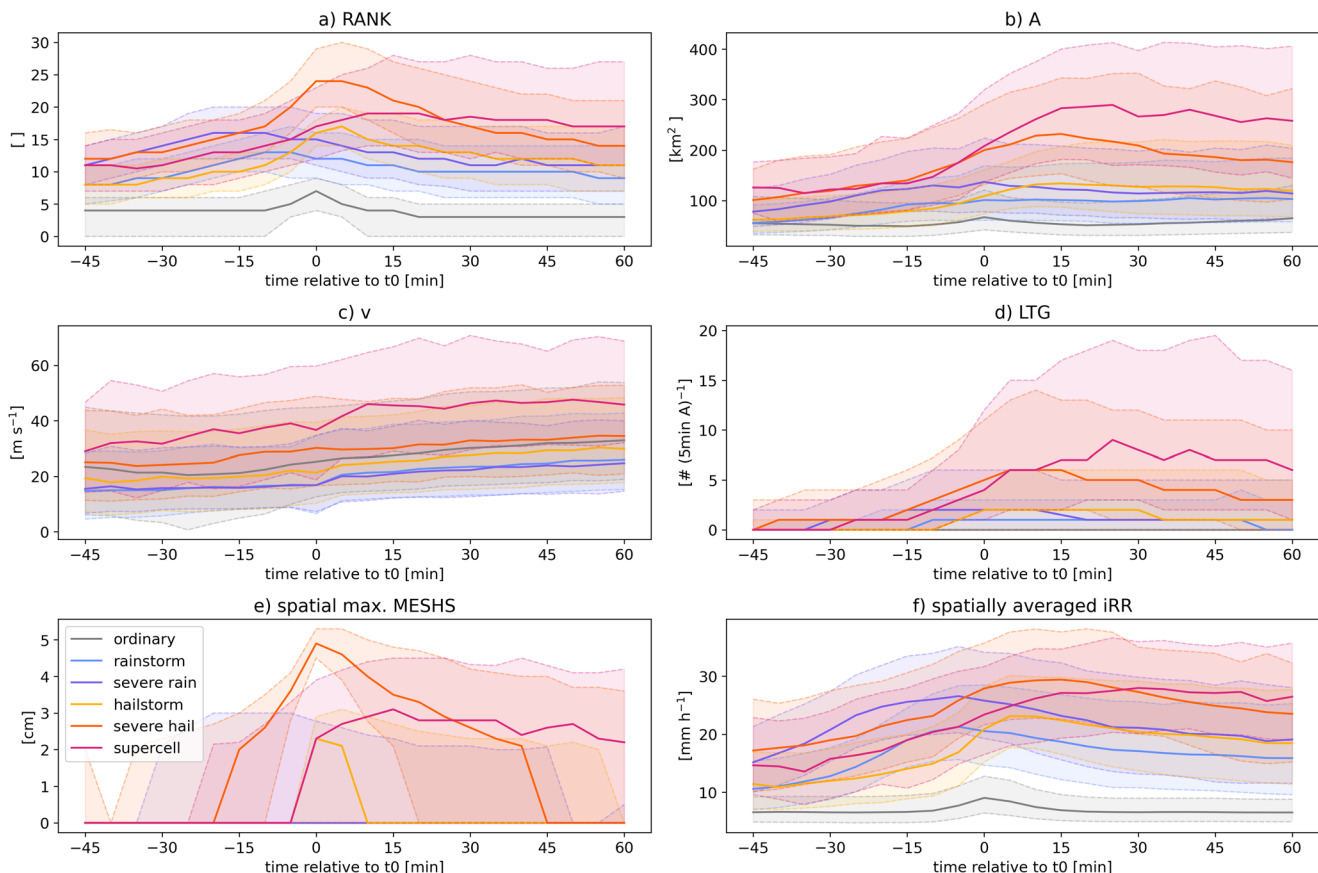


Fig. 4 Evolution of six variables during the 45 min leading up to and 60 min after the centre of the life cycle of each storm type. **a** Severity rank, **b** storm area, **c** translational speed, **d** lightning strikes, **e** maximum MESHS, **f** mean precipitation rate; the solid line depicts the median, while the shaded area represents the range of the 25th and 75th percentile.

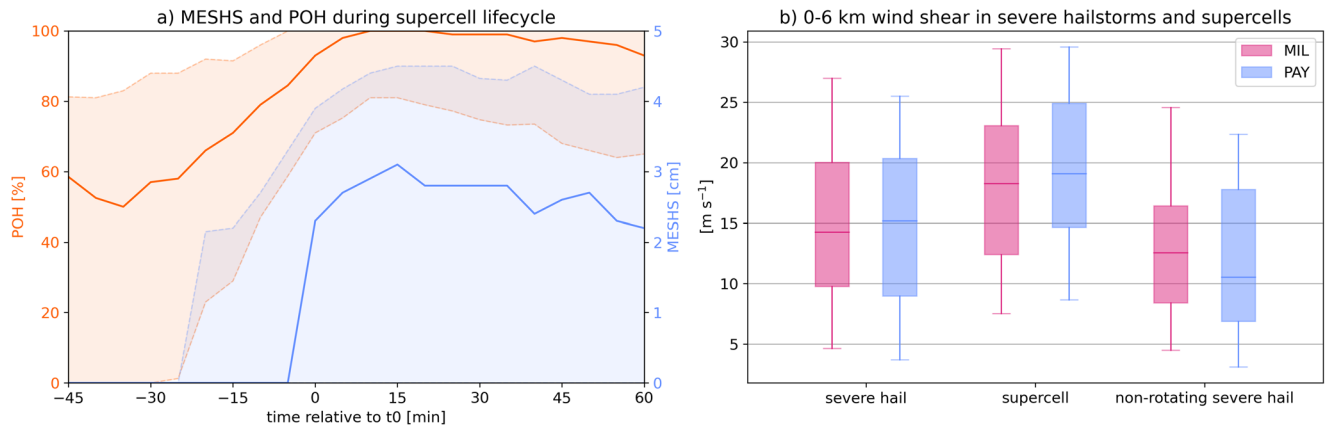


Fig. 5 Evaluating the temporal relationship between mesocyclone onset and hail. **a** Behaviour of POH and MESHS during SC life cycle; **b** deep-layer bulk shear from radiosoundings in Milano (MIL) and Payerne (PAY).

intensity peaks. As the definition of both storm types, as well as T_0 , is closely tied to MESHS, the sharp jump at T_0 is expected. We clearly see the higher, 4 cm criterion, for the SHS in comparison to the lower, 2 cm criterion, of HS. Ref. ⁸⁵ highlights the importance of the presence of rimed particles for lightning production. With riming contributing to the growth stages of HS, rimed particles are abundant. We can see a clear increase in lightning activity in HS and SHS, which is only further exceeded by SC. As also shown in ref. ²⁴, the lightning frequency increases before T_0 and peaks within the 15 min afterwards. The increase in overall severity rank, storm area, lightning rate and iRR is only shortly before T_0 . The larger area and lightning flash rates last for a longer amount of time, whereas the peaks in severity rank, MESHS and iRR are quite narrow.

SC show the overall highest peaks for A , v and LTG. With SC requiring highly sheared flow environments and also inducing motion with their internal dynamics, it is unsurprising to see the highest v here. Ref. ³⁰ also shows higher v and LTG for mesocyclonic storms in comparison to non-mesocyclonic storms in general. SC are also known to have a large spatial extent in comparison to other single storm types⁴. The peaks in the intensity-related variables tend to be broader than for HS and occur after T_0 . This shows that, as previously established in other regions, SC in our observational domain also tend to have a longer time period of peak intensity and the onset of rotation precedes the most intense phase, making it a potential nowcasting predictor for SC intensification.

The increase in translational speed over the life cycle of all storm types is notable. While the trend is small enough to lie within the quartiles, it is persistent across all types and thus covers groups of vastly different sample sizes, indicating a physical phenomenon. A similar trend was found in ref. ⁸⁴. The translational speed of most convective storms is induced by the steering flow in the mid-troposphere²¹. During convective initiation, the storm is mainly influenced by ground flow, which is generally rather low. Only once the storm extent reaches the mid-troposphere, the stronger steering flow can begin to influence the storm motion. The longer the storm experiences the influence, the more it is accelerated.

As the onset of rotation tends to precede storm intensification, we investigate the relationship with hail in more detail.

Figure 5a shows the evolution of max. MESHS and POH within the cell contours throughout the life cycle of a SC thunderstorm, with the onset of rotation occurring at T_0 . The sharp increase of MESHS at and after T_0 indicates that already falling hail tends to intensify after the detection of rotation. POH also increases with T_0 and remains elevated for approximately an hour after.

The most relevant phase for hail in a SC is during the first 30 min after the first detection of a mesocyclone. The mesocyclone detection preceding or coinciding with the onset of hail in most cases was also found in ref. ³¹, where 8 years of hailstorms were investigated in the German radar domain. This confirms the preexisting concept³⁴ that in mesocyclonic storms, the onset of the mesocyclone indicates the following onset of hail, or an increase in hail intensity, even in our observational area, where we see a large fraction of storms forming severe hail without being associated with rotation.

Contrary to other studies, most SHS in the Prealpine regions are not associated with a SC. Figure 5b shows the 0–6 km shear from soundings in Payerne and Milano for all SHS, all SC and only those SHS when no SC were present. Soundings associated with SHS, but not SC, show lower deep-layer shear, indicating that the atmospheric profile did not support the development of significant rotation on these days.

Intensity comparison of storm types in different regions

In this section, we focus on the regional differences between the different storm types. The separation into region of different orographic complexity and dominant weather regimes allows to investigate the influence of topography from an observational point of view. We look at the distribution of each variable throughout the entire life cycle of the severe storm categories (see Fig. 6). We consider 68,000 measurement points along the respective tracks for OR, 109,000 RS, 59,000 SRS, 97,000 HS, 36,000 SHS and 16,000 SC. The weaker storm categories do not show clear signals throughout the topographic regions and are represented with a summarising boxplot each.

Figure 6 shows the regional distribution of the variables RANK, A , LTG and MESHS. As a first order trend, we can observe that the more intense storm types all show higher distributions for the intensity variables than the weaker storm types. Within the severe storm types, the upper percentiles of all variables show a regional dependency, being weakest over the main Alpine ridge and increasing towards both the NW Po valley and the Swiss plateau. Particularly LTG and MESHS are stronger to the Southern side of the Alps, where hail occurs more frequently¹¹. The predominantly Mediterranean climate favours higher temperatures, CAPE and moisture content, leading to more convective activity in general⁶⁷.

The regional intensity differences are most pronounced for SC, indicating that topography has a strong impact on a SC's ability to intensify. SC exhibiting lower RANK, A , LTG and MESHS can occur in all regions. The more complex orography introduces an upper limit to the maximum possible strength of SC, and to a lesser extent SRS and SHS. The top 50 percentiles of the intensity variables consistently follow the regional pattern for SC. The bulk

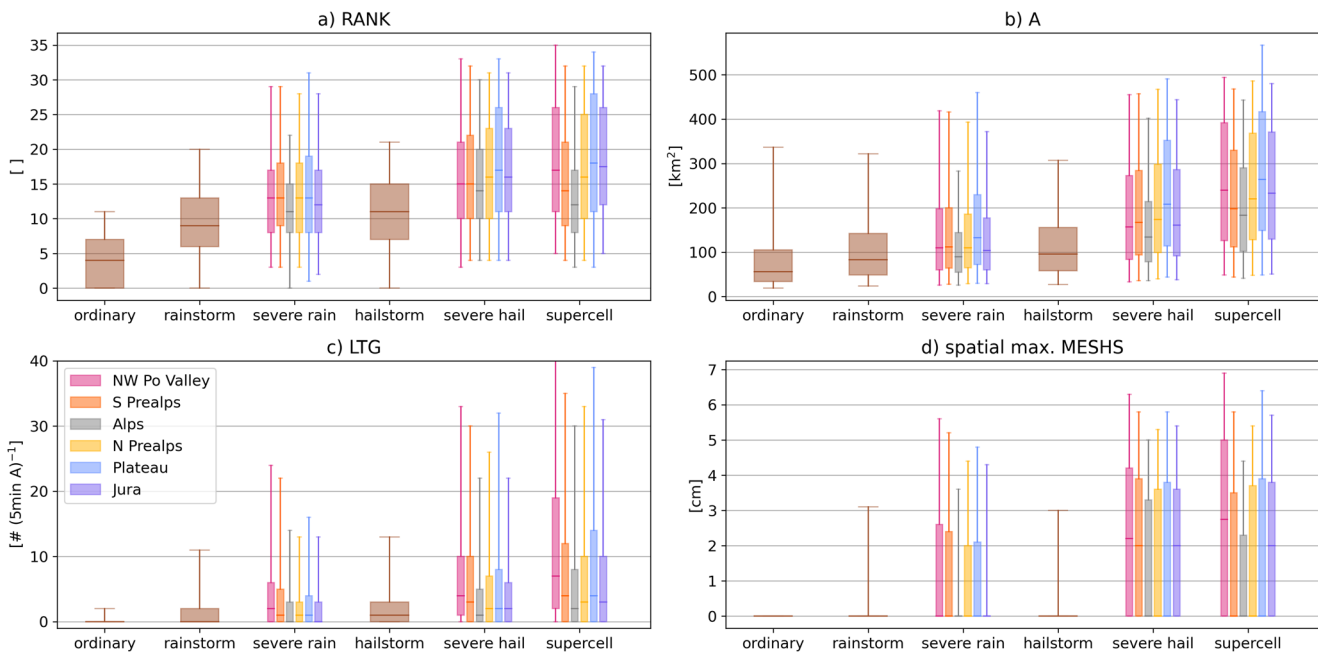


Fig. 6 Distribution of four variables for the different thunderstorm types in each topographic region. **a** Severity rank, **b** storm area, **c** lightning strikes, **d** maximum MESHS. The boxplots depict the median (centre line), 25th and 75th percentiles (bounds of box) and 5th and 95th percentiles (whiskers).

of the distributions overlaps, but the upper percentiles are consistently higher in regions of less topographic complexity. While the Prealpine regions show the highest concentration of SC tracks (see Fig. 3b), the highest severity storms on each Alpine side occur in the NW Po Valley for the South and the Swiss plateau for the North, indicating that less complex terrain favours the co-occurrence of SC ingredients and hence the intensification of the storm^{29,66}. Contrarily, the presence of moderately complex terrain in the Prealps supports the general presence of SC, even if not of the highest severity ones.

Radio-sounding data of different storm types

In Fig. 7, we investigate the atmospheric profile associated with the different storm categories. The variables CAPE, precipitable water, surface and 6-km wind speed, as well as directional and speed shear are derived from the radiosoundings in Payerne and Milano. They each represent the storm categories on the Northern and Southern side of the Alps, respectively. The Southern side of the Alps shows higher values of CAPE and, most notably, precipitable water throughout all storm categories. In addition, OR are associated with distinctly lower CAPE and precipitable water values than all other storm types. As discussed in Fig. 4c, we can see in Fig. 7c, d that all storm categories are associated with very low surface wind speeds and significantly higher flow aloft at 6 km. SRS have a tendency to lower wind speeds at 6 km, which is a contributing factor to their low translational speed (and hence high accumulation). The 6-km wind speed is highest for the SC, confirming the elevated wind shear seen in Fig. 5b).

DISCUSSION

This analysis investigates the behaviour of different convective storm types in the Alpine region. Making use of 6 years of high-quality operational radar data from a network of five radars, a systematic data set of ordinary, intense rain, hail and supercell thunderstorms is produced for the convective season of the years 2016–2021. Although 6 years is a limited timeline particularly for

events as infrequent as SC, having a homogeneous data set for all storm types allows for a direct comparison of their regional intensity and life cycles. The limitations of the radar network apply to all storm categories equally, therefore not creating biases through different observation methods. This study offers a first-time comprehensive comparison of convective storm types in different orographic regions, with an emphasis of investigating the behaviour of SC thunderstorms in complex terrain.

SC represent the most severe storm type and show considerable overlap with both RS and HS. Generally, OR show the weakest values in intensity variables, whose values increase steadily over RS and HS to SC. SC are generally associated with multiple convective hazards, their impact is compounded by the simultaneous occurrence of several severe weather phenomena, such as hail and intense rain. In contrast to previous research^{31,86}, the majority of HS (97%) and SHS (76%) in the Alpine region do not develop a mesocyclone during their life cycle, however the vast majority of storms with a mesocyclone produce hail (88%). Most SHS in the observational domain form in conditions of lower deep shear, which is unfavourable for the evolution of a sustained, rotating updraught. The discrepancy may additionally partially be owed to differences in the storm classification, as we here use purely radar-based HS and SC detection algorithms, whereas³¹ use a selection of hailstorms based on ground reports. Especially SC detection can be less reliable in complex terrain and underestimate the occurrence of shallow, low-lying rotation due to low-level beam blockage.

An initial investigation of the frequency distribution of each storm type shows that the South of the Alps is more convectively active than the North. To the South the convectively more favourable Mediterranean climate dominates. In addition, on each side of the Alps, the Prealpine areas show the highest density of convection for each storm type, indicating that moderately complex topography is beneficial to the overall presence of convection, e.g., by facilitating convective initiation.

A further analysis of the regional intensity differences shows that more complex orography usually leads to less severe storms. The peak intensities for each storm type are generally found in the

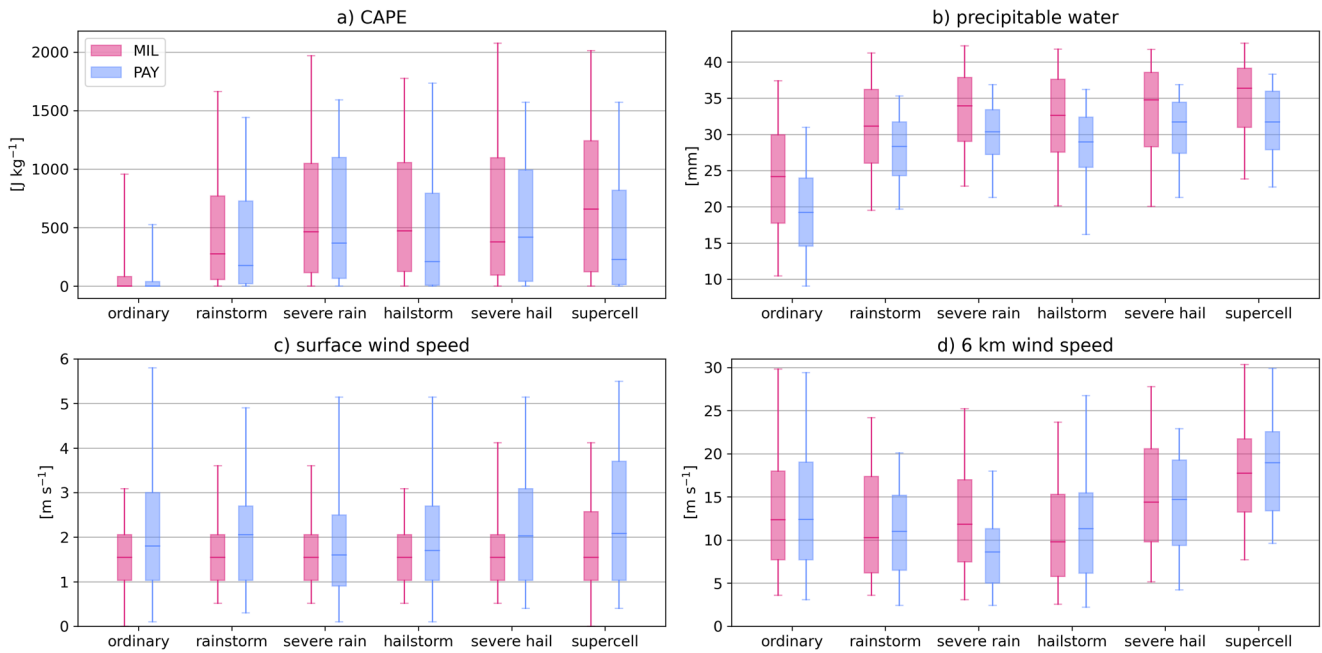


Fig. 7 Distribution of four sounding variables for the Northern and Southern Alpine regions. **a** CAPE, **b** precipitable water, **c** surface wind speed, **d** 6 km wind speed. Thunderstorms from the NW Po valley and S Prealps are assigned to the MIL sounding, while thunderstorms from the Jura, Swiss plateau and N Prealps are assigned to the PAY sounding. The boxplots depict the median (centre line), 25th and 75th percentiles (bounds of box) and 5th and 95th percentiles (whiskers).

Swiss plateau for the Northern half of the domain and the NW Po valley for the Southern half. Overall, the strongest storms are prevalent in the NW Po valley, where we also find a systematically higher precipitable water content. In contrast, the most frequent occurrence to either Alpine side is in the Prealpine areas, the Southern Prealps having a higher occurrence than the Northern. The lowest intensities and frequencies occur over the main Alpine ridge.

To understand the evolution of convective hazards in the storm life cycles, we examine the intensity evolution of the different thunderstorm types with respect to their life cycle centre. This allows us to identify temporal relationships and potential predictors for convective hazards and intensification. As RS are defined by hourly accumulation, the processes leading up to the exceeded threshold are relevant. Thus the peak intensity of the storm generally is 30 min before the threshold is crossed. HS, however, are a more instantaneous reflection of convective severity. The intensity sharply increases with the onset of hail¹¹. For the majority of storms hail is a briefly lasting phenomenon, the intensity increase peaks briefly together with the hail occurrence, before decaying again. SC on the other hand develop a mesocyclone during the formation of the updraught, before the main intensification of the storm. So we see a steady increase in intensity around the onset of rotation that peaks 15–30 min later and remains elevated for a prolonged amount of time. The longer intensity peak also reflects the typically longer lifetime of SC, as their internal storm dynamic prolongs the expected life cycle. SC in this region are also often associated with prolonged hail swaths.

While the intensity and life cycle of SC has been studied extensively in flat terrain, it is important to establish, whether these relationships also hold true in complex terrain. The Prealpine areas, where SC are most prevalent, already present with considerable topographical complexity. In contrast to expectations by regional forecasters, SC occur regularly and exhibit many of the established behaviours such as rotation preceding hail formation, and the prolonged intensity maximum.

METHODS

Thunderstorm detection

All thunderstorms within the Swiss radar domain are identified with the operational thunderstorm radar tracking (TRT) algorithm⁷³. It employs a detection with dynamic thresholds on the 2-D Cartesian maximum reflectivity field that is derived from all five radars. From each time step to the next, detected thunderstorms are advected based on the weighted average motion of the past three detections. New detections with sufficient overlap are matched to the advected past cells to establish a continuous track.

To avoid retaining a spurious number of small cells in this data set, we remove all tracks that last less than 30 min, which represents the lower end of a typical thunderstorm life cycle. In addition, thunderstorm detections below a quality index of 0.3 (as in Fig. 1b) are removed. This only concerns the outer edges of the domain. In regions of low observational quality, the observations are skewed towards more severe phenomena, as they are more likely to still be detected.

The TRT algorithm also provides a heuristic severity rank, that summarises several intensity metrics of a thunderstorm. The intensity variables in Eq. (1) are first categorised using a fuzzy logic weighting scheme for each variable before computing the rank:

$$\text{RANK} = \frac{(2 \cdot \text{VIL} + 2 \cdot \text{ET45} + \text{Zmax} + 2 \cdot \text{A57dBz})}{7} \quad (1)$$

(RANK first developed in ref. ⁷⁴, most recent version in ref. ⁸⁵)

Thunderstorm classification

The thunderstorms are classified into the categories OR, RS, SRS, HS, SHS and SC²⁹. An overview of the classification criteria is listed in Table 3. The two rainstorm and hailstorm classes and the SC overlap considerably. While OR excludes the other classes, the more severe types can overlap and thunderstorms can contribute to multiple categories, e.g., SHS and SC.

RS and SRS are defined by the radar-estimated hourly precipitation accumulation. The instantaneous precipitation rate

(IRR) is derived on a 1 km Cartesian grid, as described in refs. 87,88. In this study, we use the radar-derived hourly accumulation of precipitation (ACC). An accumulation exceeding 30 mm in the past hour in at least three connected pixels classifies a storm as RS. Accordingly, 50 mm accumulation in the past hour correspond to the SRS classification. By requiring several pixels to exceed the threshold, we avoid triggering the threshold through potential residual clutter²⁴. By using an hourly accumulation instead of an instantaneous precipitation rate, we reduce the risk of hail being mistaken for an intense precipitation event. These thresholds mirror the operational precipitation warning thresholds in thunderstorms of MeteoSwiss⁸⁹.

To classify HS and SHS, we rely on the metrics probability of hail (POH)^{90–92} and maximum expected severe hail size (MESHS)^{92,93}. To classify as HS, either POH or MESHS must exceed 80% or 2 cm, respectively, in at least five contiguous km² (see ref. 11). To classify as SHS, MESHS must exceed 4 cm in at least five contiguous km²¹¹. For both classes, one time step fulfilling the hail or severe hail criterion is sufficient to label the entire storm as a HS or SHS. This method of classifying HS and SHS was first established in ref. 25, verified against insurance data and later established as the principal method in the Swiss hail climatology¹³. While radar-based hail detection is challenging and can differ from ground-based methods, it yields a high spatio-temporal coverage that is not achieved with crowd-sourcing⁹⁴ or hail sensors⁹⁵.

SC are classified by a mesocyclone detection algorithm that identifies consistent rotation around a vertical axis from Doppler radar data²⁹. This identifies the rotating updraught, that is a core structure of a SC^{4,96}. The processing chain here includes dealiasing the Doppler data⁹⁷, computing the azimuthal derivative per radar elevation, identifying areas of elevated azimuthal shear and employing vertical and temporal continuity constraints²⁹. The procedure merges measurements from all available radars at a given location to maximise the likelihood of detecting and tracking a mesocyclone. The use of range-dependent thresholds mitigates azimuthal resolution loss with increasing distance. Shallow, low-level mesocyclones may be veiled in areas of low-level beam blockage, persistent mesocyclones with a sufficient vertical extent are reliably detected.

Lastly, OR are separated from more severe types, not divided into severe types. They are required to have less than 4 contiguous km² of either POH >80% or MESHS >2 cm, respectively, to ensure that hail is unlikely. Similarly, at most two connected pixels may exceed 30 mm precipitation accumulation. They must also not have a detected mesocyclone. Removing these intermediate strength storms that do neither meet the classification criteria from the OR nor those of HS and RS affects less than 1% of the data.

The radiosoundings are assigned to all thunderstorm classes occurring in the 2 h before or 12 h after a sounding. For the soundings in Payerne, all thunderstorms in the Jura, Swiss Plateau and N Prealps are considered, for the Milano sounding the thunderstorms of the S Prealps and NW Po Valley. The thunderstorms over the main Alpine ridge are not used in the sounding analysis as the inner Alpine profile does not necessarily correlate with either sounding. This sounding data set is then filtered by thunderstorm category. Soundings assigned to OR contain no other thunderstorm category. Soundings assigned to RS exclude SRS and those assigned to HS exclude SHS. A sensitivity analysis of the use of sounding data is presented in Supplementary Discussion 1.

Region assignment

The outlines of the regions are shown in Fig. 1. As many thunderstorms have tracks crossing multiple regions, entering or leaving the considered domain, it is necessary to anchor points to specific regions. We aim to anchor them with the

timesteps we are most interested in. An overview of the criteria are shown in Table 3. OR are assigned to the region, where they are detected most frequently, weighted by their intensity. This anchors them in the region, where they exhibited the highest intensity for the longest time. All severe types are labelled with the region where they had the most classifications of their storm type (e.g., most detected mesocyclones). Supplementary Discussion 1 contains a sensitivity discussion regarding the region assignment.

Centring the life cycle

When comparing life cycles of storm populations, the temporal progression of the storms need to be aligned to a time T₀. Per storm type, we centre the timeline around the time of highest interest (see Table 3). For OR, this is the time of peak intensity. For the more severe storm types, we centre T₀ around the first classification of the meteorological phenomenon.

DATA AVAILABILITY

The thunderstorm data set is publicly available at zenodo.org under the <https://doi.org/10.5281/zenodo.6534510>⁹⁸. The radiosounding data are available from the University of Wyoming⁷¹. The software package [metpy](https://www.metpy.org/) was used to process the radiosoundings.

Received: 17 May 2022; Accepted: 9 March 2023;

Published online: 23 March 2023

REFERENCES

- Hoepple, P. Trends in weather related disasters—consequences for insurers and society. *Weather. Clim. Extremes* **11**, 70–79 (2016).
- Pučík, T. et al. Large hail incidence and its economic and societal impacts across Europe. *Mon. Weather Rev.* **147**, 3901–3916 (2019).
- Ward, P. J. et al. Review article: natural hazard risk assessments at the global scale. *Nat. Hazards Earth Syst. Sci.* **20**, 1069–1096 (2020).
- Markowski, P. & Richardson, Y. *Mesoscale Meteorology in Midlatitudes* (Wiley-Blackwell, 2010).
- Pučík, T. et al. Future changes in European severe convection environments in a regional climate model ensemble. *J. Clim.* **30**, 6771–6794 (2017).
- Rädler, A. et al. Frequency of severe thunderstorms across Europe expected to increase in the 21st century due to rising instability. *NPJ Clim. Atmos. Sci.* **2** <https://www.nature.com/articles/s41612-019-0083-7> (2019).
- Kron, W., Löw, P. & Kundzewicz, Z. W. Changes in risk of extreme weather events in Europe. *Environ. Sci. Policy* **100**, 74–83 (2019).
- Raupach, T. H. et al. The effects of climate change on hailstorms. *Nat. Rev. Earth Environ. Sci.* **2**, 213–226 (2021).
- Allen, J. T., Tippet, M. K., Sobel, A. H. & Lepore, C. Understanding the drivers of variability in severe convection: bringing together the scientific and insurance communities. *Bull. Am. Meteorol. Soc.* **97**, ES221–ES223 (2016).
- Martius, O. et al. Challenges and recent advances in hail research. *Bull. Am. Meteorol. Soc.* **99**, ES51–ES54 (2018).
- Nisi, L., Hering, A., Germann, U. & Martius, O. A 15 year hail streak climatology for the Alpine region. *Q. J. R. Meteorol. Soc.* **144**, 1429–1449 (2018).
- Allen, J. T. et al. Understanding hail in the earth system. *Rev. Geophys.* **58**, e2019RG000665 (2020).
- NCCS. Hail Climate Switzerland—National hail hazard maps. *National Centre for Climate Services* www.hailclimatology.ch (2021).
- Gaal, L., Molnar, P. & Szolgay, J. Selection of intense rainfall events based on intensity thresholds and lightning data in Switzerland. *Hydrol. Earth. Syst. Sci.* **18**, 1561–1573 (2014).
- Panziera, L. et al. A radar-based regional extreme rainfall analysis to derive the thresholds for a novel automatic alert system in Switzerland. *Hydrol. Earth. Syst. Sci.* **20**, 2317–2332 (2016).
- Aregger, M. P. Stationary and slow-moving convection over Switzerland: a 14-year radar-based climatology. <https://occrdata.unibe.ch/students/theses/msc/326.pdf> (2021).
- Miglietta, M. M. & Davolio, S. Dynamical forcings in heavy precipitation events over Italy: lessons from the hymex sop1 campaign. *Hydrol. Earth. Syst. Sci.* **26**, 627–646 (2022).

18. Panziera, L., Germann, U., Gabella, M. & Mandapaka, P. V. Nora-nowcasting of orographic rainfall by means of analogues. *Q. J. R. Meteorol. Soc.* **137**, 2106–2123 (2011).
19. Nisi, L., Ambrosetti, P. & Clementi, L. Nowcasting severe convection in the alpine region: the coalition approach. *Q. J. R. Meteorol. Soc.* **140**, 1684–1699 (2014).
20. Wapler, K., Hengstebeck, T. & Groenemeijer, P. Mesocyclones in central Europe as seen by radar. *Atmos. Res.* **168**, 112–120 (2016).
21. Foresti, L., Sideris, I. V., Nerini, D., Beusch, L. & Germann, U. Using a 10-year radar archive for nowcasting precipitation growth and decay: a probabilistic machine learning approach. *Weather. Forecast.* **34**, 1547–1569 (2019).
22. Sideris, I. V., Foresti, L., Nerini, D. & Germann, U. Nowprecip: localized precipitation nowcasting in the complex terrain of Switzerland. *Q. J. R. Meteorol. Soc.* **146**, 1768–1800 (2020).
23. Panziera, L. & Germann, U. The relation between airflow and orographic precipitation on the southern side of the alps as revealed by weather radar. *Q. J. R. Meteorol. Soc.* **136**, 222–238 (2010).
24. Nisi, L. et al. Hailstorms in the Alpine region: Diurnal cycle, 4d characteristics, and the nowcasting potential of lightning properties. *Q. J. R. Meteorol. Soc.* **146**, 4170–4184 (2020).
25. Nisi, L., Martius, O., Hering, A., Kunz, M. & Germann, U. Spatial and temporal distribution of hailstorms in the Alpine region: a long-term, high resolution, radar-based analysis. *Q. J. R. Meteorol. Soc.* **142**, 1590–1604 (2016).
26. Barras, H. et al. Multi-day hail clusters and isolated hail days in Switzerland—large-scale flow conditions and precursors. *Weather. Clim. Dyn.* **2**, 1167–1185 (2021).
27. Houze, R. A., Schmid, W., Fovell, R. G. & Schiesser, H.-H. Hailstorms in Switzerland: left movers, right movers, and false hooks. *Mon. Weather Rev.* **121**, 3345–3370 (1993).
28. Huntrieser, H., Schiesser, H. H., Schmid, W. & Waldvogel, A. Comparison of traditional and newly developed thunderstorm indices for Switzerland. *Weather. Forecast.* **12**, 108–125 (1997).
29. Feldmann, M., Germann, U., Gabella, M. & Berne, A. A characterisation of alpine mesocyclone occurrence. *Weather. Clim. Dyn.* **2**, 1225–1244 (2021).
30. Wapler, K. Mesocyclonic and non-mesocyclonic convective storms in Germany: storm characteristics and life-cycle. *Atmos. Res.* **248**, 105186 (2021).
31. Wapler, K. The life-cycle of hailstorms: lightning, radar reflectivity and rotation characteristics. *Atmos. Res.* **193**, 60–72 (2017).
32. Kunz, M. et al. Ambient conditions prevailing during hail events in central Europe. *Nat. Hazards Earth Syst. Sci.* **20**, 1867–1887 (2020).
33. Witt, A. et al. Rapid-scan radar observations of an Oklahoma tornadic hailstorm producing giant hail. *Weather. Forecast.* **33**, 1263–1282 (2018).
34. Davies-Jones, R. A review of supercell and tornado dynamics. *Atmos. Res.* **158–159**, 274–291 (2015).
35. Peyraud, L. Analysis of the 18 July 2005 tornadic supercell over the Lake Geneva Region. *Weather. Forecast.* **28**, 1524–1551 (2013).
36. Barthlott, C. & Kirshbaum, D. J. Sensitivity of deep convection to terrain forcing over Mediterranean islands. *Q. J. R. Meteorol. Soc.* **139**, 1762–1779 (2013).
37. Manzato, A., Davolio, S., Miglietta, M. M., Pucillo, A. & Setvák, M. 12 September 2012: a supercell outbreak in ne Italy? *Atmos. Res.* **153**, 98–118 (2015).
38. Miglietta, M. M., Manzato, A. & Rotunno, R. Characteristics and predictability of a supercell during hymex sop1. *Q. J. R. Meteorol. Soc.* **142**, 2839–2853 (2016).
39. Miglietta, M. M., Mazon, J. & Rotunno, R. Numerical simulations of a tornadic supercell over the mediterranean. *Weather. Forecast.* **32**, 1209–1226 (2017).
40. Scheffknecht, P., Serafin, S. & Grubišić, V. A long-lived supercell over mountainous terrain. *Q. J. R. Meteorol. Soc.* **143**, 2973–2986 (2017).
41. Trefalt, S. et al. A severe hail storm in complex topography in Switzerland—observations and processes. *Atmos. Res.* **209**, 76–94 (2018).
42. Grazioli, J. et al. Adaptive thunderstorm measurements using C-band and X-band radar data. *IEEE Geosci. Remote. Sens.* **16**, 1673–1677 (2019).
43. Avolio, E., Nisi, L., Panziera, L., Peyraud, L. & Miglietta, M. M. A multi-sensor and modeling analysis of a severe convective storm in Lake Maggiore area (north-western Italy). *Atmos. Res.* **242**, 105008 (2020).
44. Soderholm, B., Ronalds, B. & Kirshbaum, D. J. The evolution of convective storms initiated by an isolated mountain ridge. *Mon. Weather Rev.* **142**, 1430–1451 (2014).
45. Milrad, S. M., Lombardo, K., Atallah, E. H. & Gyakum, J. R. Numerical simulations of the 2013 Alberta flood: dynamics, thermodynamics, and the role of orography. *Mon. Weather Rev.* **145**, 3049–3072 (2017).
46. LeBel, L. J., Tang, B. H. & Lazear, R. A. Examining terrain effects on an upstate new york tornado event utilizing a high-resolution model simulation. *Weather. Forecast.* **36**, 2001–2020 (2021).
47. Mulholland, J. P., Nesbitt, S. W. & Trapp, R. J. A case study of terrain influences on upscale convective growth of a supercell. *Mon. Weather Rev.* **147**, 4305–4324 (2019).
48. Lombardo, K. & Kumjian, M. R. Observations of the discrete propagation of a mesoscale convective system during RELAMPAGO-CACTI. *Mon. Weather Rev.* **150**, 2111–2138 (2022).
49. Piper, D. et al. Exceptional sequence of severe thunderstorms and related flash floods in May and June 2016 in Germany—part 1: meteorological background. *Nat. Hazards Earth Syst. Sci.* **16**, 2835–2850 (2016).
50. Mohr, S. et al. The role of large-scale dynamics in an exceptional sequence of severe thunderstorms in Europe May–June 2018. *Weather. Clim. Dyn.* **1**, 325–348 (2020).
51. Wilhelm, J. et al. Severe thunderstorms with large hail across Germany in June 2019. *Weather* **76**, 228–237 (2021).
52. Bagagli, L., Inghrosso, R. & Miglietta, M. M. Synoptic patterns and mesoscale precursors of italian tornadoes. *Atmos. Res.* **253**, 105503 (2021).
53. Feudale, L. & Manzato, A. Cloud-to-ground lightning distribution and its relationship with orography and anthropogenic emissions in the Po valley. *J. Appl. Meteorol. Climatol.* **53**, 2651–2670 (2014).
54. Kaltenboeck, R. & Steinheimer, M. Radar-based severe storm climatology for Austrian complex orography related to vertical wind shear and atmospheric instability. *Atmos. Res.* **158–159**, 216–230 (2015).
55. Katona, B. & Markowski, P. Assessing the influence of complex terrain on severe convective environments in northeastern Alabama. *Weather. Forecast.* **36**, 1003–1029 (2021).
56. Mulholland, J. P., Nesbitt, S. W., Trapp, R. J., Rasmussen, K. L. & Salio, P. V. Convective storm life cycle and environments near the Sierras De Córdoba, Argentina. *Mon. Weather Rev.* **146**, 2541–2557 (2018).
57. Katona, B., Markowski, P., Alexander, C. & Benjamin, S. The influence of topography on convective storm environments in the Eastern United States as deduced from the HRRR. *Weather. Forecast.* **31**, 1481–1490 (2016).
58. Taszarek, M. et al. A climatology of thunderstorms across Europe from a synthesis of multiple data sources. *J. Clim.* **32**, 1813–1837 (2019).
59. Murillo, E. M. & Homeyer, C. R. Severe hail fall and hailstorm detection using remote sensing observations. *J. Appl. Meteorol. Climatol.* **58**, 947–970 (2019).
60. Allen, J. T. & Tippett, M. K. The characteristics of United States hail reports. *Electron. J. Sev. Storms Meteorol.* **10**, 1–31 (2015).
61. Murillo, E. M., Homeyer, C. R. & Allen, J. T. A 23-year severe hail climatology using gridrad mesh observations. *Mon. Weather Rev.* **149**, 945–958 (2021).
62. Ashley, W. S., Haberlie, A. M. & Strohm, J. A climatology of quasi-linear convective systems and their hazards in the United States. *Weather. Forecast.* **34**, 1605–1631 (2019).
63. Haberlie, A. M. & Ashley, W. S. A radar-based climatology of mesoscale convective systems in the United States. *J. Clim.* **32**, 1591–1606 (2019).
64. Gensini, V. A. & Brooks, H. E. Spatial trends in United States tornado frequency. *NPJ Clim. Atmos. Sci.* **1**, 2397–3722 (2018).
65. Tang, B. H., Gensini, V. A. & Homeyer, C. R. Trends in united states large hail environments and observations. *NPJ Clim. Atmos. Sci.* **2**, 45 (2019).
66. Taszarek, M. et al. Severe convective storms across Europe and the united states. part i: climatology of lightning, large hail, severe wind, and tornadoes. *J. Clim.* **33**, 10239–10261 (2020).
67. Taszarek, M., Allen, J. T., Brooks, H. E., Pilguy, N. & Czernecki, B. Differing trends in United States and European severe thunderstorm environments in a warming climate. *Bull. Am. Meteorol. Soc.* **102**, E296–E322 (2021).
68. Taszarek, M., Allen, J. T., Marchio, M. & Brooks, H. E. Global climatology and trends in convective environments from era5 and rawinsonde data. *NPJ Clim. Atmos. Sci.* **4**, 2397–3722 (2021).
69. Germann, U., Boscacci, M., Gabella, M. & Sartori, M. Peak performance: radar design for prediction in the Swiss Alps. *Meteorol. Technol. Int.* **4**, 42–45 (2015).
70. Germann, U. et al. Weather radar in complex orography. *Remote Sens.* **14**, 503 (2022).
71. University of Wyoming. Upper air data—soundings. <https://weather.uwyo.edu/upperair/sounding.html> (2022).
72. Raupach, T. H. et al. Object-based analysis of simulated thunderstorms in Switzerland: application and validation of automated thunderstorm tracking with simulation data. *Geosci. Model Dev.* **14**, 6495–6514 (2021).
73. Hering, A. M., Morel, C., Galli, G., Ambrosetti, P. & Boscacci, M. Nowcasting thunderstorms in the Alpine Region using a radar based adaptive thresholding scheme. *Proc. ERAD Conference 2004* 206–211. https://www.copernicus.org/erad/2004/online/ERAD04_P_206.pdf (2004).
74. Hering, A., Germann, U., Boscacci, M. & Senesi, S. Operational nowcasting of thunderstorms in the alps during map d-phase. *Proc. ERAD Conference 2008*. https://www.researchgate.net/profile/Urs-Germann/publication/237123756_Operational_nowcasting_of_thunderstorms_in_the_Alps_during_MAP_D-PHASE/links/54d3c17c0cf246475802d28d/Operational-nowcasting-of-thunderstorms-in-the-Alps-during-MAP-D-PHASE.pdf (2008).
75. Meteorage. Publications and technical notes. <https://www.meteorage.com/resources/publications-and-technical-notes> (2022).

76. Schulz, W., Diendorfer, G., Pedebay, S. & Poelman, D. R. The European lightning location system euclid—part 1: performance analysis and validation. *Nat. Hazards Earth Syst. Sci.* **16**, 595–605 (2016).
77. Azadifar, M. et al. Evaluation of the performance characteristics of the European lightning detection network euclid in the alps region for upward negative flashes using direct measurements at the instrumented säntis tower. *J. Geophys. Res. Atmos.* **121**, 595–606 (2016).
78. Consortium for Small Scale Modelling. MeteoSwiss operational applications within COSMO. <http://www.cosmo-model.org/content/tasks/operational/meteoSwiss/default.htm#cosmo-1> (2018).
79. Punge, H., Bedka, K., Kunz, M. & Reinbold, A. Hail frequency estimation across Europe based on a combination of overshooting top detections and the era-interim reanalysis. *Atmos. Res.* **198**, 34–43 (2017).
80. Manzato, A., Serafin, S., Miglietta, M. M., Kirshbaum, D. & Schulz, W. A pan-alpine climatology of lightning and convective initiation. *Mon. Weather Rev.* <https://journals.ametsoc.org/view/journals/mwre/aop/MWR-D-21-0149.1/MWR-D-21-0149.1.xml> (2022).
81. Enno, S.-E., Sugier, J., Alber, R. & Seltzer, M. Lightning flash density in Europe based on 10 years of ATDnet data. *Atmos. Res.* **235**, 104769 (2020).
82. Bundesamt für Meteorologie und Klimatologie MeteoSchweiz. Gewitter- und blitzhäufigkeit in der schweiz. <https://www.meteoschweiz.admin.ch/wetter/wetter-und-klima-von-a-bis-z/gewitter/gewitter-und-blitzhaeufigkeit-in-der-schweiz.html> (2017).
83. Anderson, G. & Klugmann, D. A European lightning density analysis using 5 years of ATDnet data. *Nat. Hazards Earth Syst. Sci.* **14**, 815–829 (2014).
84. Zöbisch, I. Thunderstorms: life cycle analyses and nowcasting based on multi-source data; dissertation. <http://nbn-resolving.de/urn:nbn:de:bvb:19-256804> (2020).
85. Figueras i Ventura, J. et al. Analysis of the lightning production of convective cells. *Atmos. Meas. Tech.* **12**, 5573–5591 (2019).
86. Tuovinen, J.-P., Rauhala, J. & Schultz, D. M. Significant-hail-producing storms in finland: convective-storm environment and mode. *Weather. Forecast.* **30**, 1064–1076 (2015).
87. Germann, U., Galli, G., Boscacci, M. & Bolliger, M. Radar precipitation measurement in a mountainous region. *Q. J. R. Meteorol. Soc.* **132**, 1669–1692 (2006).
88. Gabella, M., Speirs, P., Hamann, U., Germann, U. & Berne, A. Measurement of precipitation in the alps using dual-polarization c-band ground-based radars, the GPM spaceborne Ku-band radar, and rain gauges. *Remote Sens.* **9**, 1147 (2017).
89. Bundesamt für Meteorologie und Klimatologie MeteoSchweiz. Beschreibung zu den gefahrenstufen. [https://www.meteoswiss.admin.ch/content/dam/meteoswiss/de/Wetter/doc/beschreibungenzudengefahrestufen.pdf](https://www.meteoschweiz.admin.ch/content/dam/meteoswiss/de/Wetter/doc/beschreibungenzudengefahrestufen.pdf) (2021).
90. Waldvogel, A., Federer, B. & Grimm, P. Criteria for the detection of hail cells. *J. Appl. Meteorol.* **18**, 1521–1525 (1979).
91. Foote, G. B., Krauss, T. W. & Makitov, V. *Hail Metrics Using Convective Radar*, Vol. 1.5 (Amer. Meteor. Soc., 2005).
92. Betschart, M. & Hering, A. Automatic hail detection at meteoswiss—verification of the radar-based hail detection algorithms poh, meshes and hail. *Arbeitsberichte der MeteoSchweiz* 59. <https://www.meteoswiss.admin.ch/content/dam/meteoswiss/en/Ungebundene-Seiten/Publikationen/Fachberichte/doc/ab238.pdf> (2012).
93. Treloar, A. B. *Vertically Integrated Radar Reflectivity as an Indicator of Hail Size in the Greater Sydney Region of Australia* (Amer. Meteor. Soc., 1998).
94. Barras, H. et al. Experiences with >50,000 crowdsourced hail reports in Switzerland. *Bull. Am. Meteorol. Soc.* **100**, 1429–1440 (2019).
95. Kopp, J. et al. The summer 2021 Switzerland hailstorms: weather situation, major impacts and unique observational data. *Weather* <https://rmets.onlinelibrary.wiley.com/doi/abs/10.1002/wea.4306> (2022).
96. Kumjian, M. R. & Ryzhkov, A. V. Polarimetric signatures in supercell thunderstorms. *J. Appl. Meteorol. Climatol.* **47**, 1940–1961 (2008).
97. Feldmann, M. et al. R2D2: a region-based recursive Doppler dealiasing algorithm for operational weather radar. *J. Atmos. Ocean Technol.* **37**, 2341–2356 (2020).
98. Feldmann, M., Hering, A., Gabella, M. & Berne, A. Radar-based severe thunderstorm classification in Switzerland. *Zenodo* (2022).
99. @swisstopo. DhM25/200m. <https://www.swisstopo.admin.ch/de/geodata/height/dhm25200.html> (2005).
100. Jarvis, A., Reuter, H., Nelson, A. & Guevara, E. Hole-filled srtm for the globe version 4. *cgiaar-csi srtm 90m Database* <http://srtm.csi.cgiar.org> (2008).

ACKNOWLEDGEMENTS

We thank MeteoSwiss for co-funding the collaborative research between MeteoSwiss and EPFL. In addition, we are grateful for the advice and suggestions of Dr. Luca Nisi and Dr. Ulrich Hamann. *Inclusion statement:* This research was conducted as a collaboration between the Swiss federal technological university EPFL and the Swiss national weather service MeteoSwiss, both local to the Alpine region that is the focus of this study.

AUTHOR CONTRIBUTIONS

This research has been conducted by Monika Feldmann as part of her PhD projects under the supervision of Prof. Alexis Berne and Dr. Marco Gabella. Dr. Alessandro Hering has provided invaluable expertise on the use of TRT data and severe thunderstorm metrics in the Swiss radar network.

COMPETING INTERESTS

The authors declare no competing interests.

ADDITIONAL INFORMATION

Supplementary information The online version contains supplementary material available at <https://doi.org/10.1038/s41612-023-00352-z>.

Correspondence and requests for materials should be addressed to Monika Feldmann.

Reprints and permission information is available at <http://www.nature.com/reprints>

Publisher's note Springer Nature remains neutral with regard to jurisdictional claims in published maps and institutional affiliations.



Open Access This article is licensed under a Creative Commons Attribution 4.0 International License, which permits use, sharing, adaptation, distribution and reproduction in any medium or format, as long as you give appropriate credit to the original author(s) and the source, provide a link to the Creative Commons license, and indicate if changes were made. The images or other third party material in this article are included in the article's Creative Commons license, unless indicated otherwise in a credit line to the material. If material is not included in the article's Creative Commons license and your intended use is not permitted by statutory regulation or exceeds the permitted use, you will need to obtain permission directly from the copyright holder. To view a copy of this license, visit <http://creativecommons.org/licenses/by/4.0/>.

© The Author(s) 2023